Journal Pre-proofs

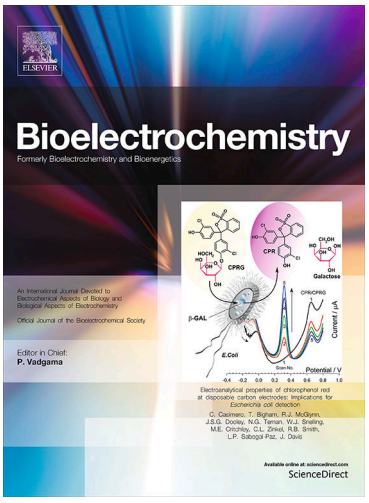

Dimanganese trioxide (Mn_2O_3) based label-free electrochemical biosensor for detection of Aflatoxin-B1

Avinash Kumar Singh, Tarun Kumar Dhiman, GBVS Lakshmi, Pratima R. Solanki

PII: S1567-5394(20)30607-1
DOI: https://doi.org/10.1016/j.bioelechem.2020.107684
Reference: BIOJEC 107684

To appear in: *Bioelectrochemistry*

Received Date: 25 May 2020
Revised Date: 3 October 2020
Accepted Date: 5 October 2020

Please cite this article as: A. Kumar Singh, T. Kumar Dhiman, G. Lakshmi, P.R. Solanki, Dimanganese trioxide (Mn_2O_3) based label-free electrochemical biosensor for detection of Aflatoxin-B1, *Bioelectrochemistry* (2020), doi: https://doi.org/10.1016/j.bioelechem.2020.107684

Dimanganese trioxide (Mn_2O_3) based label-free electrochemical biosensor for detection of Aflatoxin-B1

Avinash Kumar Singh[1,2], Tarun Kumar Dhiman[1], GBVS Lakshmi[1], Pratima R. Solanki[1*]
[1] Special Centre for Nanoscience, Jawaharlal Nehru University (JNU), New Delhi-110067, India
[2]School of Physical Sciences, JNU, New Delhi-110067, India
*Corresponding author email: partima@mail.jnu.ac.in; pratimarsolanki@gmail.com

Abstract

This work presents, a manganese oxide nanoparticles (Mn_2O_3nps) based electrochemical immunosensor for the detection of Aflatoxin-B1 (AFB1). X-ray spectroscopy study confirms the purily synthesized Mn_2O_3nps with an average crystallite size of 31.5 nm. Transmission electron microscopy study confirms average particle size of 45 nm. To fabricate an electrochemical biosensing, a thin film of Mn_2O_3nps was fabricated onto indium tin oxide (ITO) surface using electrophoretic technique. Such fabricated thin film was utilized to immobilize Anti-AFB1, antibodies for selective detection of AFB1 using differential pulse voltammetry technique. Prior to perform sensing, bovine serum albumin (BSA) is utilized to block the uncovered sites on the BSA/Anti-AFB1/Mn_2O_3/ITO immunoelectrode surface. The response of BSA/Anti-AFB1/Mn_2O_3/ITO immunoelectrode was measured as a function of AFB1 in a linear detection range of 1 pg mL^{-1} to 10 µg mL^{-1} and sensor showed highest sensitivity of 2.044 µA mL $ng^{-1}cm^{-2}$ with lower detection limit of 0.54 pg mL^{-1}. A spiked sample response of corn extract was studied in the linear range of 1 pg mL^{-1} to 10 µg mL^{-1} and immunoelectrode (BSA/Anti-AFB1/Mn_2O_3/ITO) showed recovery rate of 98.6 %.

Keywords: Aflatoxin B1; co-precipitation; electrophoretic; immunoelectrode; Mn_2O_3nps.

1. Introduction

Manganese (Mn), the 12th most common element, is a vital component of metabolism and works as a cofactor in various enzymatic activities. The oxide forms of Mn i.e. MnOx are considered as a transitional material and their development as nanosystems are emerging as a potential platform for developing nano-enabled opto-electric systems. Researchers have synthesized different compositions of MnOx such as manganese oxide (MnO), dimanganese trioxide (Mn_2O_3), manganese dioxide (MnO_2), and trimanganese tetraoxide (Mn_3O_4) of varies morphology involving nanoparticles, nanorods, nanowires etc., depending on targeted application. Each form of MnOx nanomaterials has shown remarkable application in various field due to promising and tunable properties including paramagnetism, semiconducting nature and undergo phase transition.[1-4] Among various MnOx nanostructured MnO_2 and Mn_3O_4 are widely being used in various fields, such as pharmaceutical industries, biomedical applications, air decontamination agents, magnetic material, supercapacitor, and catalysts due to biocompatibility and tunable novel properties.[5,6] Among all forms, nanostructured Mn_2O_3 emerged as a potential nano-structured suitable for biosensor platform but not well explored.

Mn_2O_3 is p-type semiconductor of direct bandgap nanomaterial of 4.2 eV and has been considered for various semiconductor industry/research as associated with electrochemical sensors/biosensors, photo-catalysts, supercapacitors and lithium-ion batteries.[1,7,8,9,10] Moreover, Mn_2O_3 nps possess sufficient binding sites for adsorption of biomolecules including antibodies, protein and DNA, which are required for biosensor fabrications. Chen et al., 2015, reported synthesis of Mn_2O_3 hollow nanospheres and its use for non-enzymatic electrochemical sensor fabrication for hydrogen peroxide (H_2O_2) detection.[11] In another study, Mn_2O_3 nanofibers with the bandgap of 1.2-1.29 eV range were fabricated and used for the development of atrazine electrochemical immunosensor.[12] Authors have reported that the Mn_2O_3 has sufficient capacity to transfer electrons at electrode/electrolyte interface resulting

in enhanced sensitivity and lower limit of detection of sensors. Mn_2O_3 nanofibres were also used for dengue virus detection using DNA primers.[13] Therefore, Mn_2O_3 nanomaterial provides wide scope for the electrochemical immunosensor fabrication for other analytes, including mycotoxins.

Mycotoxins are naturally occurring secondary fungal metabolite compounds that led to biochemical, physiological, and pathological changes in animals, plants, and other species. Among various mycotoxins, Aflatoxin B1 (AFB1) is the most prevalent and potent form of these toxins.[14] International Agency for Research on Cancer also classified AFB1 as a group I carcinogen.[15] Hence, from a health perspective, AFB1 detection is significant and requires advanced and fast measurable equipment that can give quick results. Several conventional methods like enzyme-linked immunosorbent assay, high-performance liquid chromatography, liquid chromatography-mass spectroscopy, etc. have been employed for the detection of AFB1. However, they have many complications such as tough to handle, costly equipment requirements and longer turn around time etc thus, restricting their use at mass scale. Therefore, the most suitable detection methods of AFB1 with low cost and easy to handle equipment is the electrochemical biosensor. Few research groups reported electrochemical immunosensor for AFB1 detection using different nanomaterials. Solanki et al., have developed an immunosensor based on bismuth oxide nanorods (nBi_2O_3) for the detection of AFB1.[16] Chauhan et al., developed a reusable piezoelectric immunosensor for the detection of AFB1 based on gold-coated iron oxide core-shell nanoparticles. The reusability was achieved by forming a sandwiched system in which gold-coated iron oxide nanoparticles were used to tag secondary rabbit-immunoglobulin antibodies.[17] The 3D gold nanoparticle (AuNPs) coated quartz crystal microbalance based (EQCM) piezoelectric immunosensor for the detection of AFB1 was reported.[18] Singh et al., have developed an immunosensor based on rare earth samarium oxide nanorods ($n\text{-}Sm_2O_3$) for the detection of AFB1.[19] Srivastava et al., have

developed an immunosensor for the detection of AFB1 using electrochemically deposited reduced graphene oxide (RGO) platform.[20] Sharma et al., developed an immunosensor for the detection of AFB1 using cysteamine (Cys) functionalized-AuNPs.[21]Kalita et al., used the ring-like self-assembled Ni nanoparticles (RnNi) platform based immunosensor for the detection of AFB1.[22] Ma et al., developed a chitosan-AuNPs based immunosensor for the detection of AFB1.[23] A self-assembled monolayer of lipoic acid functionalized electrodes obtained from recordable compact disks (CD-trode) was used for the development of immunosensor to detect AFB1.[24] A complex gold electrode modified by a biocompatible film of multiwall-carbon nanotubes (CNTs)/poly (diallyl dimethyl ammonium chloride) (PDDA)/ Pd–AuNPs immunosensor for the detection of AFB1 was developed by Zhang et al..[25] Pan et al., reported nanobodies (Nb-70) based immunosensor, it is different approach for the detection of AFB1. Nanobodies were immobilized on prussian blue functionalized graphene oxide (GO-PB) and an ammonolysis product of 3,4,9,10-perylenetetra carboxylic dianhydride (PTC-NH_2)-AuNPs onto glassy carbon electrode (GCE).[26] Table 1 shows comparative data of previously reported findings and present work. In all of these studies, either complex electrode fabrication steps or costly materials like AuNPs were used for the development of the immunosensor for AFB1 detection.

Keeping above mentioned into consideration, this research if focussed on exploring a cost-effective and efficient electrochemical immunosensing platform. The cubic phase Mn_2O_3nps was synthesized using a co-precipitation method. These Mn_2O_3nps were characterized using various techniques including X-ray diffraction (XRD), High-resolution transmission electron microscope (HR-TEM), scanning electron microscopy (SEM) and electrochemical techniques. These Mn_2O_3nps were electrophoretically deposited onto indium tin oxide (ITO) coated glass substrate and used for immobilization of antibodies specific to AFB1 (Anti-AFB1). The blocking agent bovine serum albumin (BSA) was used to block the non-binding

sites of electrode to avoid the background signal. This BSA/Anti-AFB1/Mn_2O_3/ITO immunoelectrode exhibits the wide detection range and found good agreement with the spiked samples result. In the present study, pure phase Mn_2O_3NPs were synthesized by calcination at 550 ^oC, which is very low temperature as compared to the temperatures (900 ^oC) reported in the literature. This out comes of this research are claimed as the first report projecting an immunosensor based on Mn_2O_3 nanoparticles for the detection of mycotoxins.

Table 1. Comparison of the current study with the previously reported results

Electrode	**Technique**	**Detection range** (ng mL^{-1})	**Sensitivity**	**LOD** (ng mL^{-1})	**Ref**
BSA/Ab-AFB1/nBi_2O_3/ITO	CV	0.01–0.7	1.132 µA ng^{-1} dL cm^{-2}	0.087	16
Cys/AuNPs/HDT/Au	EQCM-CV	1–10	126 µA ng^{-1} mL cm^{-2}	0.008	18
BSA/Ab-AFB1/n-Sm_2O_3/ITO	CV	0.01–0.7	48.39 µA pg^{-1} mL^{-1} cm^{-2}	0.057	19
anti-AFB1/RGO/ITO	CV	0.125–1.5	68 µA ng^{-1} mL cm^{-2}	0.12	20
BSA/aAFB1-C-AuNP/MBA/Au	CV, DPV	0.1–1	0.45 µA ng^{-1}dL	0.179	21
a-AFB1/DMSO/RnNi-film/ITO	CV	0.05–1	0.59 µA ng^{-1}dL	0.327	22
Anti-AFB1/chitosan-AuNPs	CV	0.2–30	72.34 µA ng^{-1} mL cm^{-2}	0.12	23
Au CD-trode	EIS	1.56–31.2	-	0.34	24
AFB1/CNTs/PDDA/Pd-Au	CV	0.05–25	-	0.03	25
BSA/NB-70/GO-PB-PTC-NH_2-AuNps/GCE	DPV	0.01–100	-	0.0033	26
BSA/anti-AFB1/AuNPs/PEDOT/ITO	DPV	1–25	3.72 µA ng^{-1} mL	0.0045	27
Streptavidin-ALP/Anti-AFB1/SPCE	LSV	0.15–2.5	-	0.15	28
IgG/AFB1-BSA	LSV	0.1–10	-	0.06	29
GC/polyNeutral Red/ Poly carboxy latedthiacalix[4] arene A	DPV	0.03–31	-	0.03	30
BSA/Anti-AFB1/Mn_2O_3/ITO	DPV	0.001–10000	2.044 µA mL ng^{-1} cm^{-2}	0.00055	*This work*

HDT: 1,6-hexanedithiol; MBA: 4-mercaptobenzoic acid; DMSO: dimethyl sulfoxide; Pd-Au: palladium-gold; PEDOT:Poly(3,4-ethylene dioxythiophene); Streptavidin-ALP:Streptavidin Alkaline Phosphatase; IgG: Immunoglobulin-G; GCE: glassy carbon electrode; PTC-NH_2 (an ammaonolysis product of 3,4,9,10-perylene tetracarboxylic dianhydride); NB-70 nanobody against AFB1. SPCE: screen-printed carbon electrode; EIS: electrochemical impedance spectroscopy; LSV: linear sweep voltammetry.

2. Methods and Materials

2.1 Reagents

Manganese acetate tetrahydrate (99.99 %) and sodium hydroxide (98 %) were purchased from Sigma-Aldrich and Fisher Scientific, respectively. Indium Tin Oxide (ITO) coated glass substrate was purchased from Baltracom, UK, with 1.1 mm thick, and sheet resistance of 25 Ω sq^{-1}. Antibodies specific to aflatoxin-B1 (Anti-AFB1) were purchased from Abcam, USA, whereas antigen aflatoxin-B1 (AFB1), ochratoxin-A(OTA), fumonisin-B1 (FU-B1) and bovine serum albumin (BSA) were obtained from Sigma Aldrich.

2.2 Synthesis of Manganese oxide nanoparticles

Manganese oxide nanoparticles (Mn_2O_3nps) were synthesized using a co-precipitation method. This method has many advantages over other methods. It is easy to handle and requires minimal equipment. The nanoparticles size can be controlled by various parameters such as precursor concentration, reducing agent type, and its concentration, reaction temperature, and calcination temperature in the post-processing. All these factors make this method an ideal for the low-cost synthesis of Mn_2O_3nps.[31,32,33] Manganese acetate tetrahydrate (0.1M) and sodium hydroxide (0.25M) were used as a precursors and reducing agent, respectively. Sodium hydroxide was added drop by drop to manganese acetate under constant stirring of 300 rpm till the pH of the solution reached pH~12. Thenthe precipitate was filtered out using Whatman filter paper and washed several times using D.I water to neutralize the pH and bring it to pH~7. The obtained precipitate was dried in the oven at 80 °C overnight followed by grinding using a mortar-pestle to get afine powder of Mn_2O_3nps and then calcined at 550 °C for 4 h. Scheme 1 is showing the synthesis process of Mn_2O_3nps with the corresponding reactions.

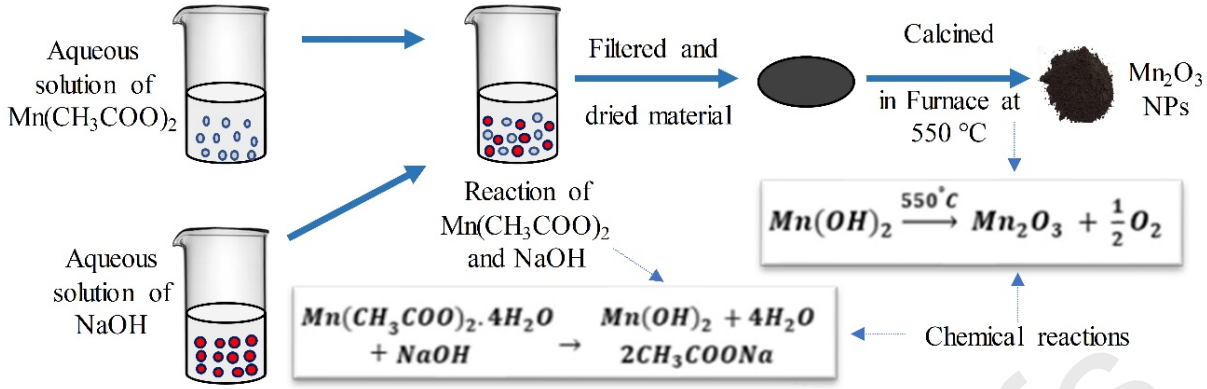

Scheme 1: Synthesis process of Mn_2O_3nps using co-precipitation method; Boxes show the corresponding chemical reactions.

2.3 Characterization Techniques

X-ray diffraction (XRD, RigakuMiniFlex 600 X-Ray Diffractometer with CuKα radiation at λ=1.54Å) working prameters are 40 kV Voltage, 15 mA current. XRD pattern of the samples were obtained in the 2θ range of 20˚-70˚ at a scan rate of 4˚ per minutes with a step size of 0.02˚. Raman spectra were recorded using Enspectr R 532 in the range of 250-1250 cm^{-1} using a 532 nm green laser. The morphology of the material was examined by field emission scanning electron microscope [(FE-SEM): MIRA II LMH from TESCAN], with a resolution of 1.5 nm at 30 kV. The elemental composition of nanomaterial was analyzed by energy-dispersive X-ray diffractiondetector (INCA PentaFET3) with 133 eV resolution from OXFORD instruments.The high-resolution transmission electronmicroscopy (HR-TEM) (JEOLJEM-2200 FS, Japan) imaging was carried out toidentify the crystallographic structure of Mn_2O_3nps. Mn_2O_3nps were ultrasonically dispersed in absolute isopropyl alcohol and deposited onto ITO coated glass through electrophoretic deposition (EPD) method. Fourier transform infrared (FTIR-Perkin-Elmer Spectrum 1) spectroscopy was used to study the streaching and bending vibration of Mn_2O_3nps and confirm its functionalization with Anti-AF-B1 and BSA. Electrochemical studies were performed using a single-channel electrochemical analyzer (Autolab-AUT-Metrohm). Cyclic voltammetry (CV) and

differential pulse voltammetry (DPV) were used to study the electro-kinetics, and electrochemical measurements, respectively, in 0.1M phosphate buffer saline (PBS, pH 7.0) containing 5 mM $[Fe(CN)_6]^{3-/4-}$ as redox species.

2.4 Fabrication of Mn_2O_3/ITO electrode using EPD

First, ITO coated glass substrates were cleaned using a mixture of H_2O:NH_3:H_2O_2 in the ratio of 5:1:1 by putting the substrates in the oven for 1 hour at 80 °C for hydrolysis. The ITO substrates were rinsed using deionized water and ethanol, followed by dring at 60 °C for 1 hour. The Mn_2O_3 films were prepared on the ITO coated glass substrate using EPD technique.[34] This technique was chosen because it produces a uniform and reproducible films. The Mn_2O_3 solution (1 mg/mL) prepared in isopropyl alcohol, followed by ultrasonication was prepared for the EPD process. For thin film prepartation, 50 µL of Mn_2O_3 solution was added in 3 mL of acetonitrile solution and 60 Volts potential for 5 minutes was applied on ITO coated glass substrate.

2.5Immunoelectrode fabrication Steps

For immunoelectrode fabrication, a solution of 5% Anti-AFB1 (in sodium phosphate buffer), EDC (0.4 M) and NHS (0.1 M) were freshly prepared in the ratio of 2:1:1 and kept it for 1 h at 4 ºC. During the immobilization, 20 µL solution of activated EDC-NHS (COO^- group of the Anti-AFB1) was uniformly drop casted on the surface of Mn_2O_3/ITO electrode and kept it in the humid chamber for 6 h at room temperature (25 ºC). An electrostatic interaction takes place between the carbonyl group of Anti-AFB1 and positively charged Mn_2O_3nps resulting in metal esterbond formation (Scheme 2).[35] The unbound Anti-AFB1 was washed out using saline sodium phosphate buffer (pH 7.0) from the Anti-AFB1/Mn_2O_3/ITO bioelectrode surface. Blocking of non-specific sites on bioelectrode (Anti-AFB1/Mn_2O_3/ITO) was performed by utilizing BSA (10 µL) and incubation was done for 4 h at 25 ºC in humid chamber. Thus finally, BSA/Anti-AFB1/Mn_2O_3/ITO immunoelectrode was washed with PBS

buffer (pH 7.0) and stored at 4 ºC for further study. The fabrication steps of BSA/Anti-AFB1/Mn_2O_3/ITO immunoelectrode is shown in Scheme 2.

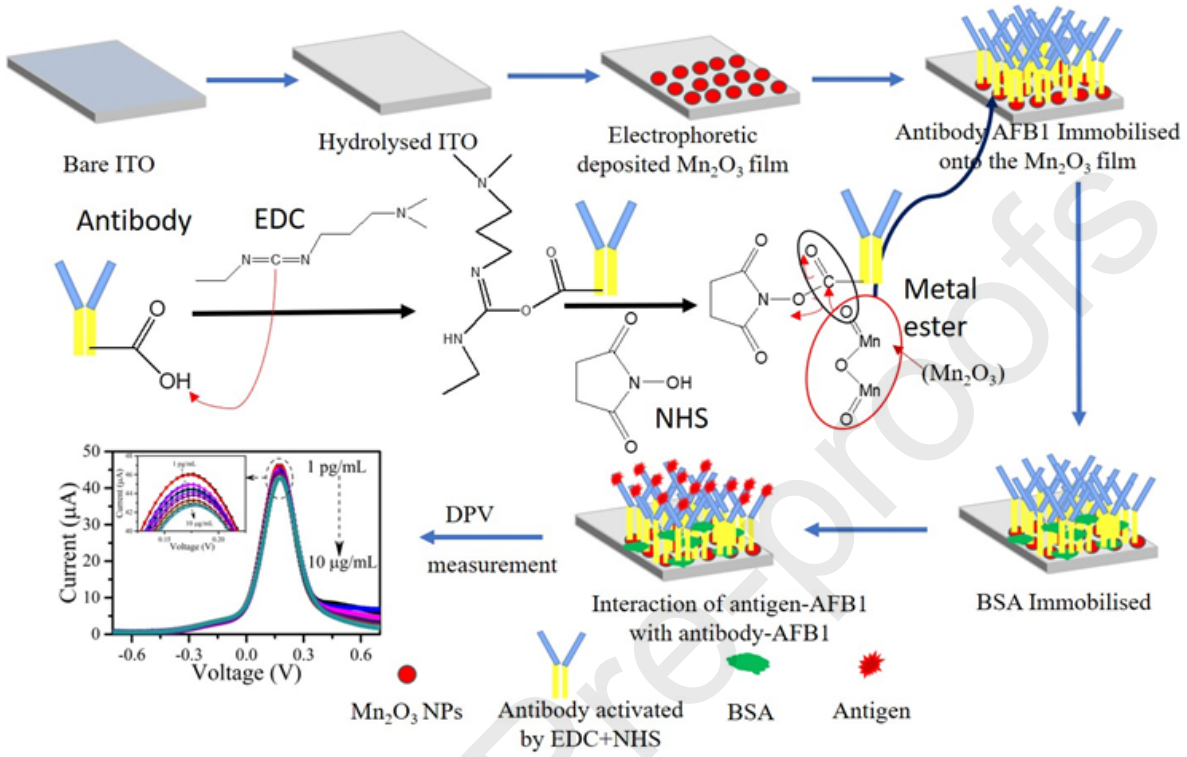

Scheme 2: Hydrolyzation of ITO coated glass, immobilization of Anti-AFB1 and BSA on the Mn_2O_3nps deposited on ITO surface and DPV measurement.

3. Results and Discussion

3.1 Structural analysis using XRD and Raman spectroscopy

XRD spectrum of Mn_2O_3nps was recorded at room temperature to determine the crystal structure and phase purity [Figure 1 (a)]. XRD pattern of the Mn_2O_3nps matched perfectly with JCPDF no. 89-4836, indicating the formation of a pure phase of Mn_2O_3nps. The diffraction peaks were found at 32.86°, 38.12°, 45.05°, 49.32°, 53.27°, 55.08°, 60.63°, 64.02°, 65.67°, and 67.34° and indexed as (222), (400), (322), (431), (521), (440), (611), (541), (622) and (136). The structure of Mn_2O_3nps was found to be cubic with the Ia3 space

group. In this structure, the unit cell is perfectly cubic without any defects. The average crystallite size was calculated using Debye-Scherrer formulae as given below:

$$D = \frac{K\lambda}{\beta \cos(\theta)} \quad \text{(i)}$$

where K~0.9; wavelength (λ) = 1.5406 Å; full width at half maximum (FWHM) of the diffraction peaks is β, and the Bragg's diffraction angle is θ.[36] Using the above formulae, the average crystallite size was found to be 31.5 nm. The average crystallite size was calculated for four peaks positioned at 22°, 32°, 55°, and 66°. Raman study was performed further to understand the phase purity and surface defects in the material.

Raman spectrum of Mn_2O_3nps was recorded using a 532 nm green laser. Raman spectrum of Mn_2O_3nps was fitted with Lorenz function to obtain the various Raman modes. Figure 1 (b) shows four peaks centered around 280, 346, 632, and 695 cm^{-1}. According to group theory, Mn_2O_3nps has 22 Raman active modes.[37]Although most of these Raman active modes are not seen in Mn_2O_3nps due to the non-polarization. In the cubic structure of Mn_2O_3nps with the Ia3 space group, the major peaks are centered around 340 and 690 cm^{-1}.[38] Peaks at 280 and 346 cm^{-1} are due to the bending vibration of the Mn-O bond. The peaks at 632 cm^{-1} and 695 cm^{-1} are due to thestretching vibration in the Mn-O bond in Mn_2O_3.[39-42] Since, the four peaks are ascribed to the known Raman active modes of Mn_2O_3, therefore it is concluded that no impurity was present. These results confirm the formation of pure cubic structure of Mn_2O_3nps. Also, surface defects are absent in Mn_2O_3nps, showing no- non-stoichiometry based effects.

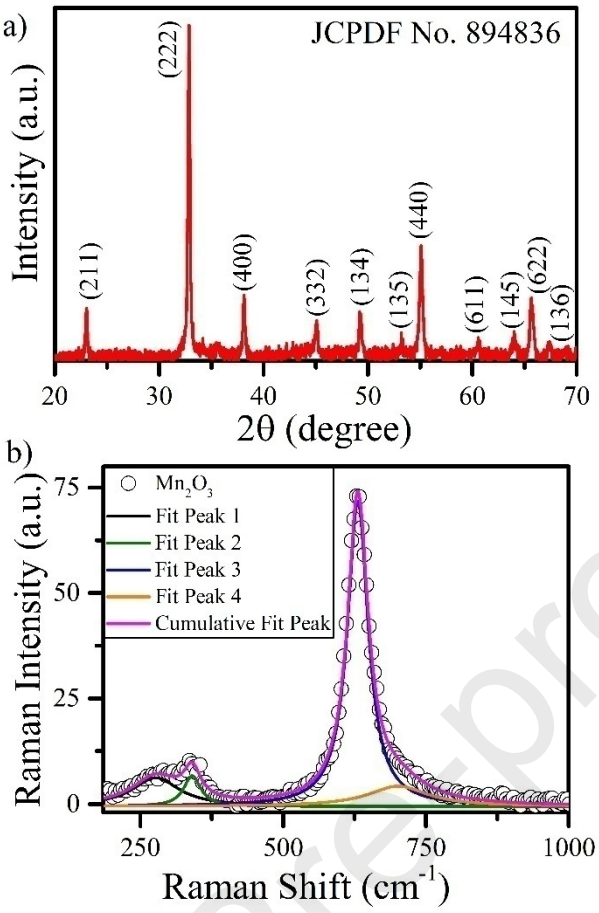

Fig. 1. (a) XRD patterns of Mn_2O_3 and (b) Raman spectra of Mn_2O_3nps

3.2 Elemental composition and morphology study of the Mn_2O_3 nps

FE-SEM image [Figure 2(a)] clearly represents small size and nearly spherical shape of the Mn_2O_3nps. The elemental composition analysis of Mn_2O_3nps was carried out using EDX technique, as shown in Figure 2 (a) and (b). EDX confirms the presence of manganese and oxygen atom in Mn_2O_3nps composition, without presence of any residues. The weight and atomic percentages were obtained as 23.28 % and 51.02 % for oxygen and 76.72 % and 48.98 % for manganese, respectively, which confirms the purity of Mn_2O_3nps.

TEM was performed to study the morphology and crystallinity of Mn_2O_3nps. Figure 2 (c) and (d) revealed approximately spherical shape of Mn_2O_3nps with an average size between 20-30 nm. Figure 2(e) shows the selected area electron diffraction (SAED) patterns. It can be clearly seen from the image (e) that each ring has been constructed over a set of points

forming a ring which are corresponding to different planes. It is known that in magnetic nanomaterials, the electron diffraction patternis not same as ring structure as obtained in other semiconducting nanomaterials, because of magnetic field interference (i.e. diffracted electron before reaching the detector). The d-spacing of these rings was calculated using the following formulae:

$$D = \frac{L\lambda}{R} \quad \text{(ii)}$$

Where D is the d spacing, L is the camera length (0.2 m), λ is the wavelength of the electron beam, R is the radius of the ring in SAED pattern. With the help of XRD data, the d-spacing and the corresponding planes were matched. Using the above formulae, four concentric diffraction rings were indexed having planes (211), (222), (332), and (440). These results are in agreement with the XRD results. Figure 2(f) shows the HR-TEM image and d-spacing was found to be 3.9 Å. The d-spacing obtained from HR-TEM corresponds to the (211) plane of the cubic phase of Mn_2O_3nps. FE-SEM, EDX,and TEM studies have confirmed the nanocrystalline nature of the Mn_2O_3nps without any trace of impurity.

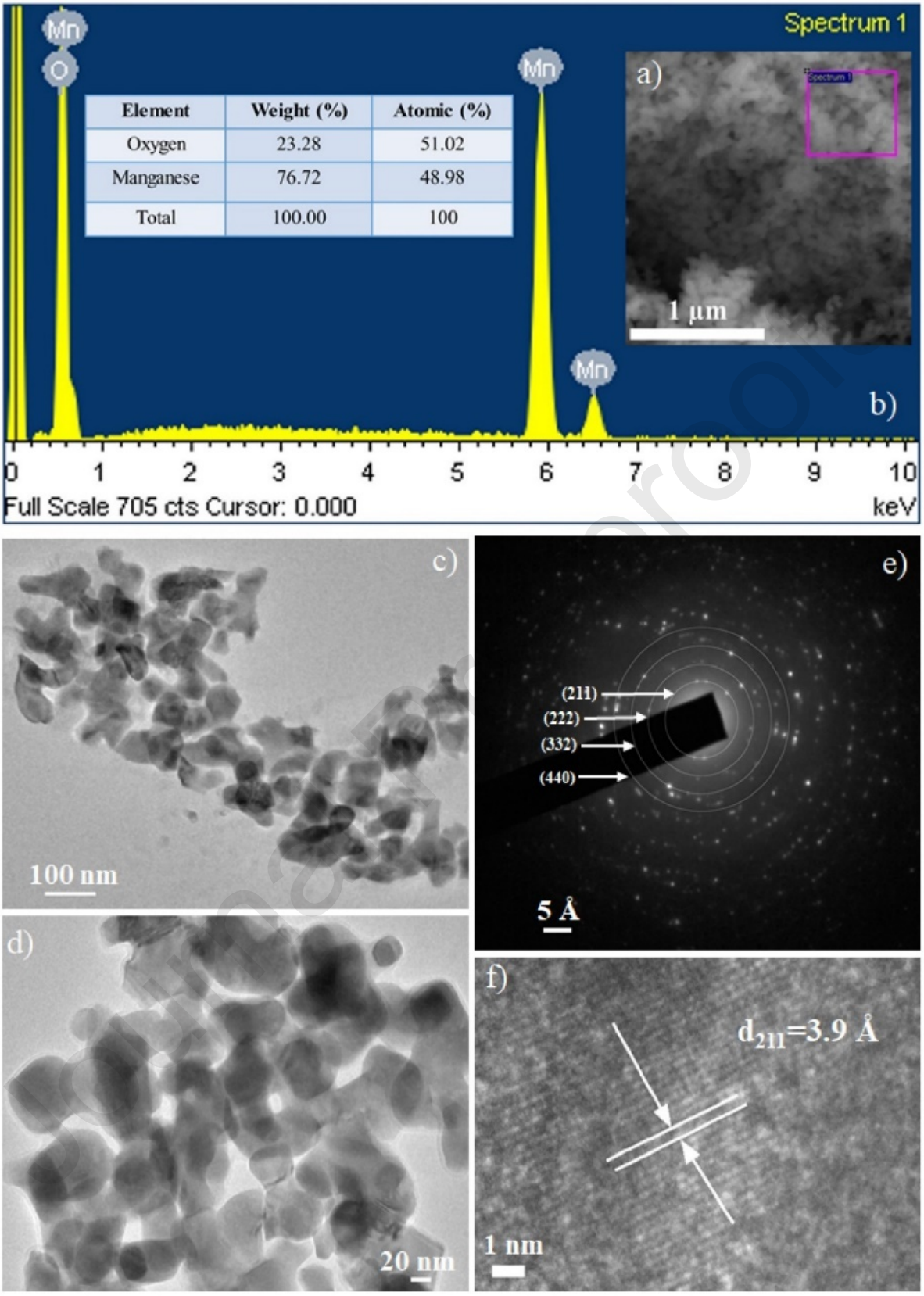

Fig.2. (a), (b) SEM and EDX image, respectively; (c) and (d) TEM images; (e) SAED pattern and (f) HR-TEM image of Mn_2O_3nps.

3.3 FTIR Study

The FTIR studies were carried out to monitor the Mn_2O_3nps formation and immobilization of Anti-AFB1 and BSA onto the Mn_2O_3/ITO electrode (Figure 3). Figure 3 (a) represents the FTIR spectrum of Mn_2O_3/ITO electrode showing small peaks at 585, and 778 cm^{-1}, corresponds to the Mn-O bond while two other small peaks at 854 and 1101 cm^{-1} assigned to O-H hydroxyl peak connected with Mn atom.[43,44]The FTIR spectrum for Ab/Mn_2O_3/ITO shows a peak at 1066 cm^{-1} representing the C-N (C-NH_2) stretching vibration of primary amine while the peak at 1456 cm^{-1} attributes the anti-symmetric CH_3 deformation and another sharp peak at 1630 cm^{-1} ascribed the amino acid (NH^{3+}) deformation.[46] These results represent the successful immobilization of Anti-AFB1 onto the Mn_2O_3/ITO electrode because the intensity of Mn_2O_3nps peaks gets reduced. IR peaks of Mn-O bond disappeared after the immobilization of BSA onto the Anti-AFB1/Mn_2O_3/ITO immunoelectrode. It was also observed that there is not any change in peak wavenumber of but having less intensity, which confirms the blocking of nonspecific sites by BSA.

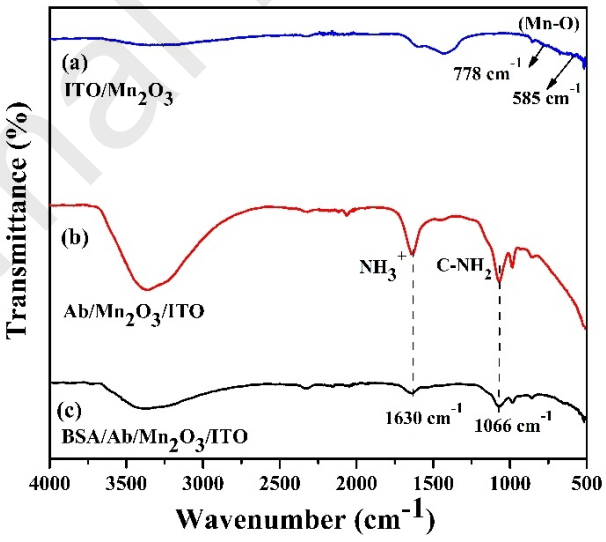

Fig.3. FTIR spectra of (a) Mn_2O_3/ITO electrode, (b) Anti-AFB1/Mn_2O_3/ITO and (c) BSA/Anti-AFB1/Mn_2O_3/ITO immunoelectrode

3.4 Electrochemical Study

3.4.1 pHand incubation time study

The change in the electrolyte pH (PBS buffer containing $[Fe(CN)_6]^{3-/4-}$ redox species) affects the electrochemical response of BSA/Anti-AFB1/Mn_2O_3/ITO immunoelectrode [Figure 4 A(a)]. DPV response was measured by varying pH inrange of 6.0 - 8.0 with potential range of -0.7 to +0.7 V. The structural behavior of Anti-AFB1 and BSA immobilized onto Mn_2O_3/ITO electrode can be disturbed due to the change in the pH. The maximum peak current was observed at pH 7.0. The obtained result shows that the highest activity of Anti-AFB1 occurred at neutral pH 7.0. To control the acidic or alkaline effect surrounding the whole Anti-AFB1 response was performed at neutral pH 7.0 because alteration in H^+ or OH^- ions present in the buffer solution may denature the Anti-AFB1.

Figure 4A (b) shows the incubation study, where incubation time was recorded at 5 min interval. DPV technique was used to perform the incubation time study for the interaction of AFB1 with the BSA/Anti-AFB1/Mn_2O_3/ITO immunoelectrode in PBS buffer (pH 7.0) containing $[Fe(CN)_6]^{3-/4-}$, keeping fixed concentration of AFB1 (1 pg mL^{-1}). The peak current recorded for BSA/Anti-AFB1/Mn_2O_3/ITO immunoelectrode was decreased and saturated after 30 minutes. Thus, 30 minutes was considered as the optimized incubation time for the AFB1 to react with Anti-AFB1 immobilized on the surface of BSA/Anti-AFB1/Mn_2O_3/ITO immunoelectrode.

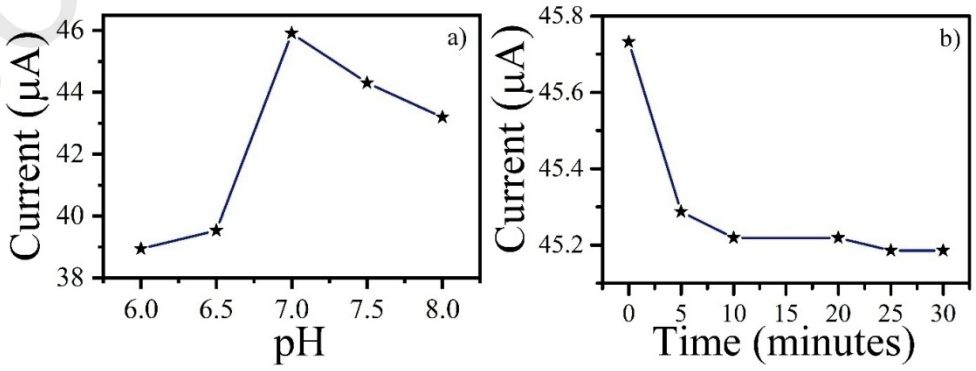

Fig.4 A. (a) The effect of pH and (b) incubation time for the electrochemical response of BSA/Anti-AFB1/Mn_2O_3/ITO immunoelectrode in PBS (0.1 M; 7 pH) containing $[Fe(CN)_6]^{3-/4-}$.

3.4.2 Electro-kinetic study

Electro-kinetics studies were performed using the CV technique in the scan rate range of 10 to 100 mV s^{-1} for the Mn_2O_3/ITO electrode, Anti-AFB1/Mn_2O_3/ITO, and BSA/Anti-AFB1/Mn_2O_3/ITO immunoelectrodes at the electro-analytical interface [Figure 4B (a-d)]. The anodic (Ia) and cathodic (Ic) current ratio was calculated at 50 mVs^{-1} for Mn_2O_3/ITO electrode [curve (a)], Anti-AFB1/Mn_2O_3/ITO [curve (b)], and BSA/Anti-AFB1/Mn_2O_3/ITO immunoelectrodes [curve (c)]. Inset Figure 4B (a,b,c) shows the plot between sqaure root of scan rate v/s peak current (Top) and sqaure root of scan rate v/s peak voltage (bottom). The peak current ratio (Ia/Ic) for Mn_2O_3/ITO electrode, Anti-AFB1/Mn_2O_3/ITO, BSA/Anti-AFB1/Mn_2O_3/ITO immunoelectrodes were obtained as 1.16, 1.17 for and 1.15, respectively thus representing the quasi-reversible electron process. In electro-kinetic studies, peak potential separation was calculated using relation ΔEp = Epa-Epc, where Epa and Epc represent anodic and cathodic peak potential. The ΔEp value for BSA/Anti-AFB1/Mn_2O_3/ ITO immunoelectrode was found as 0.371 V, which is higher in comparision with Anti-AFB1/Mn_2O_3/ITO immunoelectrode, indicating an efficient electron transfer between immunoelectrode and redox species.

Diffusion controlled process of BSA/Anti-AFB1/Mn_2O_3/ITO immunoelectrode was estimated by a simultaneous increase of anodic (Ia) and cathodic (Ic) current with the square root of scan rate during electro-analytical interaction at the interface shown in Figure 4 B(c). The diffusion coefficient (D_f) of immunoelectrode at the interface of electrolyte was calculated using Randles–Sevcik equation which is given below:

$$Ip = (2.69 \times 10^5) Cn^{3/2} D^{1/2} v^{1/2} A \qquad \text{(iii)}$$

Where Ip indicates the peak current, v is scan rate, A is the area of immunoelectrode, C is the concentration of redox probe, and n is the number electron participated.[44] The calculated diffusion coefficient for immunoelectrode BSA/Anti-AFB1/Mn_2O_3/ITO immunoelectrode was 9.15×10^{-12} cm^2 s^{-1}, which indicates a higher rate of electron transfer at the electro-analytical interface. In order to determine the maximum binding sites available at the surface of immunoelectrode, the value of Ae was calculated using the relation of Randles–Sevcik equation, and the above-calculated diffusion coefficient value was also used in the calculation. The relation is as follows:

$$A_e = \frac{S}{(2.69 \times 10^5) n^3 c D^{1/2}} \quad \text{(iv)}$$

Where S is a slope of straight line obtained from the plot of Ipa versus scan rate, and other symbols are same as mentioned in the above equation. The higher value of *Ae* was observed around 6.67 mm^2, which shows the presence of more binding sites at the BSA/Anti-AFB1/Mn_2O_3/ITO immunoelectrode per unit volume. Moreover, the surface concentration of ionic species (I* in $mol.cm^{-2}$) for the corresponding immunoelectrode was calculated using Brown-Anson equation, as stated below

$$I_p = \frac{n^2 F^2 I^* A V}{4 R T} \quad \text{(v)}$$

Where F stands for Faraday constant (96485 C mol^{-1}), T is the temperature (300 K), R is the gas constant (8.314 J mol^{-1} K^{-1}), and other symbols have the same meaning as mentioned in the previous equation. The higher value of I* (1.95×10^{-5} mol cm^{-2}) for BSA/Anti-AFB1/Mn_2O_3/ITO immunoelectrode indicates the higher concentration of reactive species at the interface.[47]

Figure 4B (d) shows the comparisonof DPV plot for Mn_2O_3/ITO electrode, Anti-AFB1/Mn_2O_3/ITO, and BSA/Anti-AFB1/Mn_2O_3/ITO immunoelectrodes. The peak current of the Mn_2O_3/ITO electrode increased after the immobilization of Anti-AFB1 and decreased

upon further immobilization of BSA. The current increase upon Anti-AFB1 immobilization is due to the interaction between the Mn_2O_3 and Anti-AFB1 interface, which became a conducting path for the charge carriers at the interface.[34] Further, the unbound sites were blocked by BSA led to a decrease in the peak currentas BSA is insulating in nature. A slight shift in peak voltage was also observed after incorporation of BSA, indicating the successful immobilization. The comparison in DPV and CV peak current values for Mn_2O_3/ITO electrode, Anti-AFB1/Mn_2O_3/ITO, and BSA/Anti-AFB1/Mn_2O_3/ITO immunoelectrodes are given in Table 2.

Table 2.Comparison in DPV peak current for Mn_2O_3/ITO electrode, Anti-AFB1/Mn_2O_3/ITO, and BSA/Anti-AFB1/Mn_2O_3/ITO immunoelectrodes.

S.N.	Electrode	DPV peak current at 50 mV/s (μA)	DPV Voltage at 50 mV/s	CV peak current at 50 mV/s (μA)	CV Voltage at 50mV/s
1	Mn_2O_3/ITO	37.84	0.1617	189.63	0.288
2	Anti-AFB1/Mn_2O_3/ITO	50.62	0.1617	252.8	0.286
3	BSA/Anti-AFB1/Mn_2O_3/ITO	45.28	0.1768	227.38	0.301

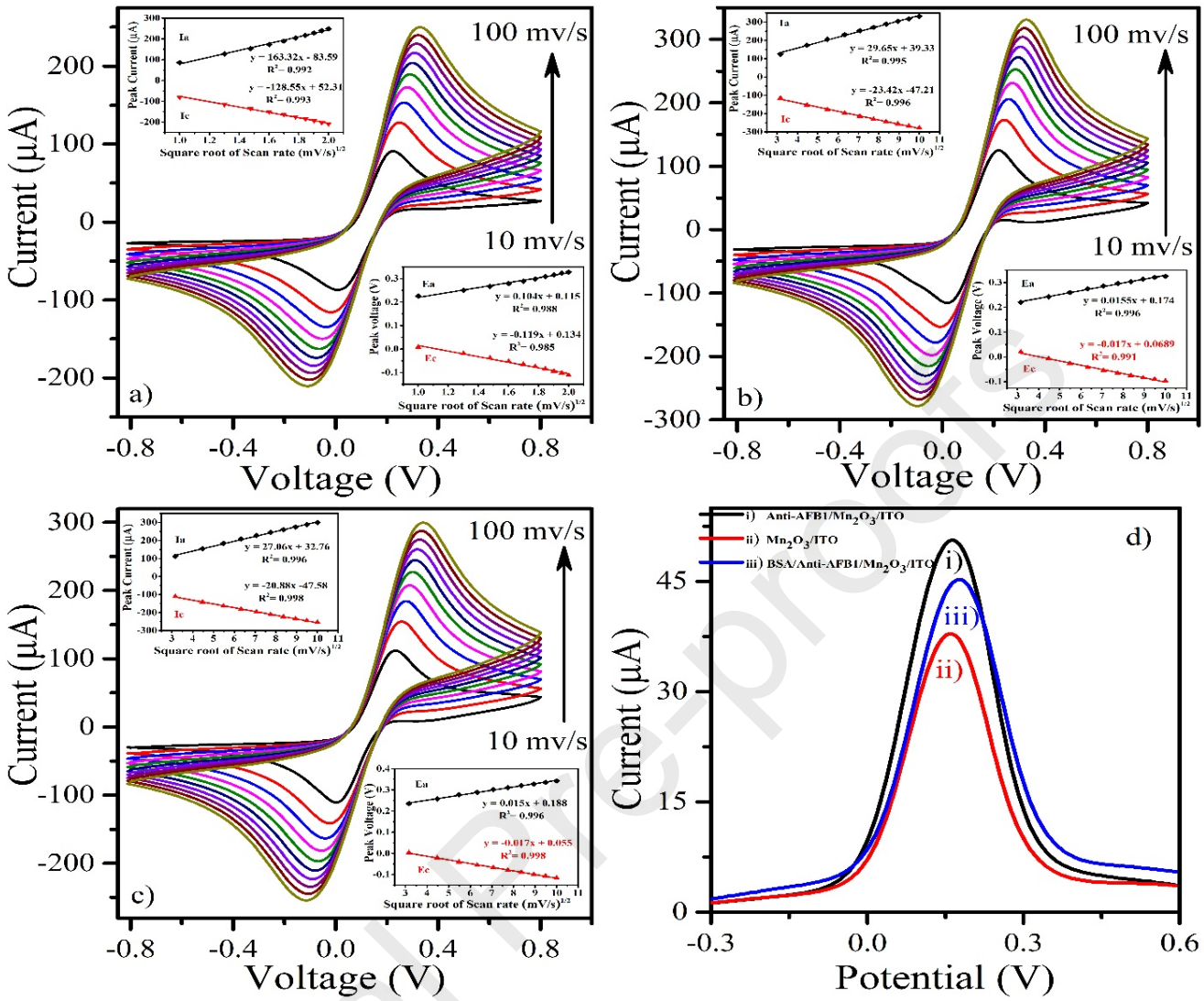

Fig. 4B Scan rate study and linear plot of (a) Mn_2O_3/ITO, (b) Anti-AFB1/Mn_2O_3/ITO, (c) BSA/Anti-AFB1/Mn_2O_3/ITO; Inset figure (a,b,c) shows the plot between sqaure root of scan rate v/s peak current (Top) and sqaure root of scan rate v/s peak voltage (bottom); (d) DPV response for Mn_2O_3/ITO electrode, Anti-AFB1/Mn_2O_3/ITO and BSA/Anti-AFB1/Mn_2O_3/ITO immunoelectrodeinPBS (0.1 M; 7 pH) containing $[Fe(CN)_6]^{3-/4-}$.

3.4.3 Electrochemical Response study of Immunoelectrode

Figure 5(a) shows the electrochemical response of BSA/Anti-AFB1/Mn_2O_3/ITO immunoelectrode against AFB1 with varying concentrations in a range of 1 pg mL^{-1} to 10 µg mL^{-1}. These results were recorded in the potential range from -0.7 to 0.7 V. The value of current decreases continuously with the varying concentration of AFB1 [Figure 5 (b)], due to the binding of AFB1 with the Anti-AFB1 at the electrode surface. This immunocomplex

formation [AFB1/BSA/Anti-AFB1/Mn_2O_3/ITO immunoelectrode] inhibits the charge transfer between BSA/Anti-AFB1/Mn_2O_3/ITO immunoelectrode and electrolytic solution $[Fe(CN)_6]^{3-/4-}$. The response of BSA/Anti-AFB1/Mn_2O_3/ITO immunoelectrode was recorded in the presence of AFB1 spiked sweet corn sample, in the same concentrations range (1 pg mL^{-1} to 10 μg mL^{-1}) [Fig. 5(c)]. The percentage of recovery for the spiked sample was obtained between 95 % to 98.6 %, and the relative standard deviation (RSD) value for each was calculated and shown in Table 3.

The linear plot between Anti-AFB1 concentration and ΔI value, and AFB1 spiked sweet corn sample and ΔI value is shown in Figure 5(d). The linear response of BSA/Anti-AFB1/Mn_2O_3/ ITO immunoelectrode against non-spiked and AFB1 spiked corn samples was recorded in the concentration range from 1 pg mL^{-1} to 10 μg mL^{-1}. The sensitivity for both the samples was calculated according to the following formulae:

$$S = \frac{Slope}{Area\ of\ the\ film} \quad \text{(vi)}$$

The sensitivity for the non-spiked sample, was found to be 2.044 μA mL $ng^{-1}cm^{-2}$ with a regression coefficient (R^2) of 0.959. The sensitivity for the AFB1 spiked corn sample was found to be 1.484 μA mL $ng^{-1}cm^{-2}$ with R^2 of 0.953. The limit of detection (LOD) was calculated using the formula; LOD = 3σ/m, where σ indicates standard deviation of blank samples and m indicates the slope of a linear plot. LOD for non- spiked samples was observed as 0.54 pg mL^{-1}. However, LOD for AFB1 spiked corn samples was found as 0.58 pg mL^{-1}.

The BSA/Anti-AFB1/Mn_2O_3/ITO immunoelectrode showed good linearity in both the AFB1 (non-spiked) and AFB1 spiked corn samples with high sensitivity. The recovery (%) obtained from AFB1 sweet corn sample using BSA/Anti-AFB1/Mn_2O_3/ITO immunoelectrode was calculated using formula % Recovery = peak current of spiked corn sample/peak current of

AFB1(non-spiked) *100. The % recovery was achieved in the range of 95.6-98.6 % (Table 3).

These results also imply that BSA/Anti-AFB1/Mn_2O_3/ITO immunoelectrode showed good linear response for the detection of AFB1 in real samples withina broad range.

Table 3. Recovery of AFB1 from sweet corn sample using BSA/Anti-AFB1/Mn_2O_3/ITO immunoelectrode and comparison of peak current between immunoelectrode and spiked sample.

S.No.	AFB1 concentrations (ng mL^{-1})	Peak current measured from DPV against AFB1 samples	Peak current measured from DPV against corn spiked samples	Relative standard deviation (RSD %)	Recovery (%)
1	0.0001	46.05	44.34	2.68	96.28
2	0.01	45.95	43.94	3.16	95.62
3	0.1	44.95	43.88	1.70	97.61
4	1	44.92	43.67	2.0	97.21
5	10	44.49	43.09	2.26	96.85
6	100	43.82	42.35	2.41	96.64
7	1000	42.87	42.30	0.95	98.67
8	10000	42.60	41.80	1.44	98.1

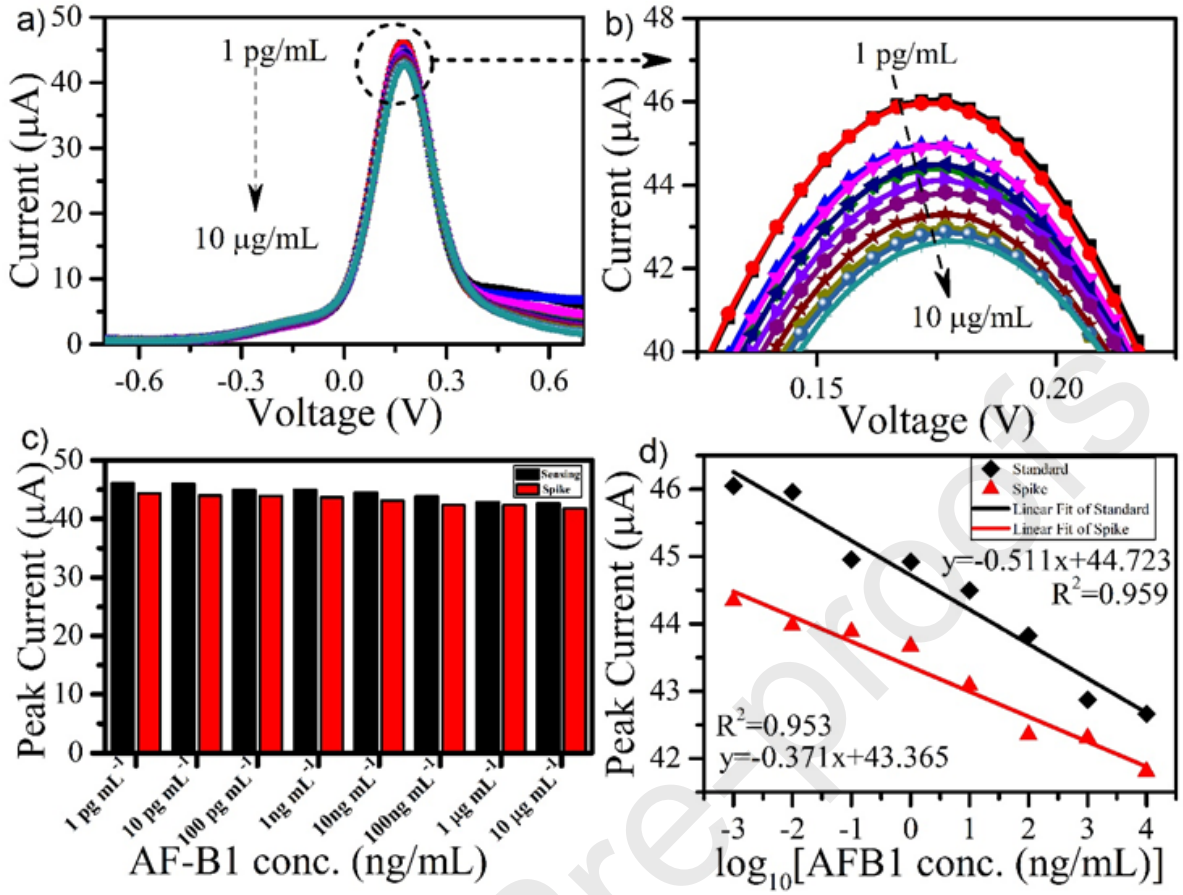

Fig. 5 (a) DPV response study of BSA/Anti-AFB1/Mn_2O_3/ITO immunoelectrode (b) zoom plot of response study (c) bar plot of spiked and immunoelectrode and (d) linear plot of BSA/Anti-AFB1/Mn_2O_3/ITO immunoelectrode and spiked sample in PBS (0.1 M; 7 pH) containing $Fe(CN)_6]^{3-/4-}$.

3.4.4 Reproducibility, repeatability, control and interference Studies

Reproducibility of five replicate immunoelectrodes (BSA/Anti-AFB1/Mn_2O_3/ITO) were monitored using DPV technique. Figure 6(a) shows a bar graph of different immunoelectrodes with high reproducibility and a relative standard deviation of 2.77 %. This measurement was recorded for 5 ng mL^{-1} concentration based immunoelectrode and almost stable current was observed, which confirmed the reproducibility and stability of the immunosensor.

Figure 6(b) shows a repeatability study of 1 ng mL^{-1} concentration based immunoelectrode (BSA/Anti-AFB1/Mn_2O_3/ITO) using DPV technique. Six consective readings were taken

which showed very less changes in peak current values. These two studies have shown the highly reproducible and repeatable nature of the BSA/Anti-AFB1/Mn_2O_3/ITO immunoelectrodes.

The control study was performed to check the role of Mn_2O_3/ITO (without Anti-AFB1) with different concentrations of Anti-AFB1 varying from 1 pg mL^{-1} to 10 μg mL^{-1} under the similar conditions which was followed for BSA/Anti-AFB1/Mn_2O_3/ITO immunoelectrode. Figure 6 (c) shows the continuous increase of ΔI as the concentration increases from 1 pg mL^{-1} to 1 ng mL^{-1} and then decreased for remaining concentrations. Thus, this study represented that Mn_2O_3/ITO did not appropriately interact with AFB1 in the absence of Anti-AFB1.

Figure 6 (d) shows the interference study of BSA/Anti-AFB1/Mn_2O_3/ITO immunoelectrode against various interferants such as corn, maize, oleaginous fruits, and cereals. This study was performed on the immunoelectrode BSA/Anti-AFB1/Mn_2O_3/ITO using DPV technique. The specificity of immunoelectrode was analysed with different mycotoxin species, like OTA and FU-B1. Besides this, other chemicals which are naturally present in food (D-glucose, cellulose, and starch) were also studied as interferant. During the selectivity test, 15 μL of each interferants (mycotoxins and chemicals) were added into the electrolyte solution in the presence of AFB1 and monitored the response with DPV. Results obtained ascribed the high selectivity for AFB1 with BSA/Anti-AFB1/Mn_2O_3/ITO immunoelectrode against various interferants**.**

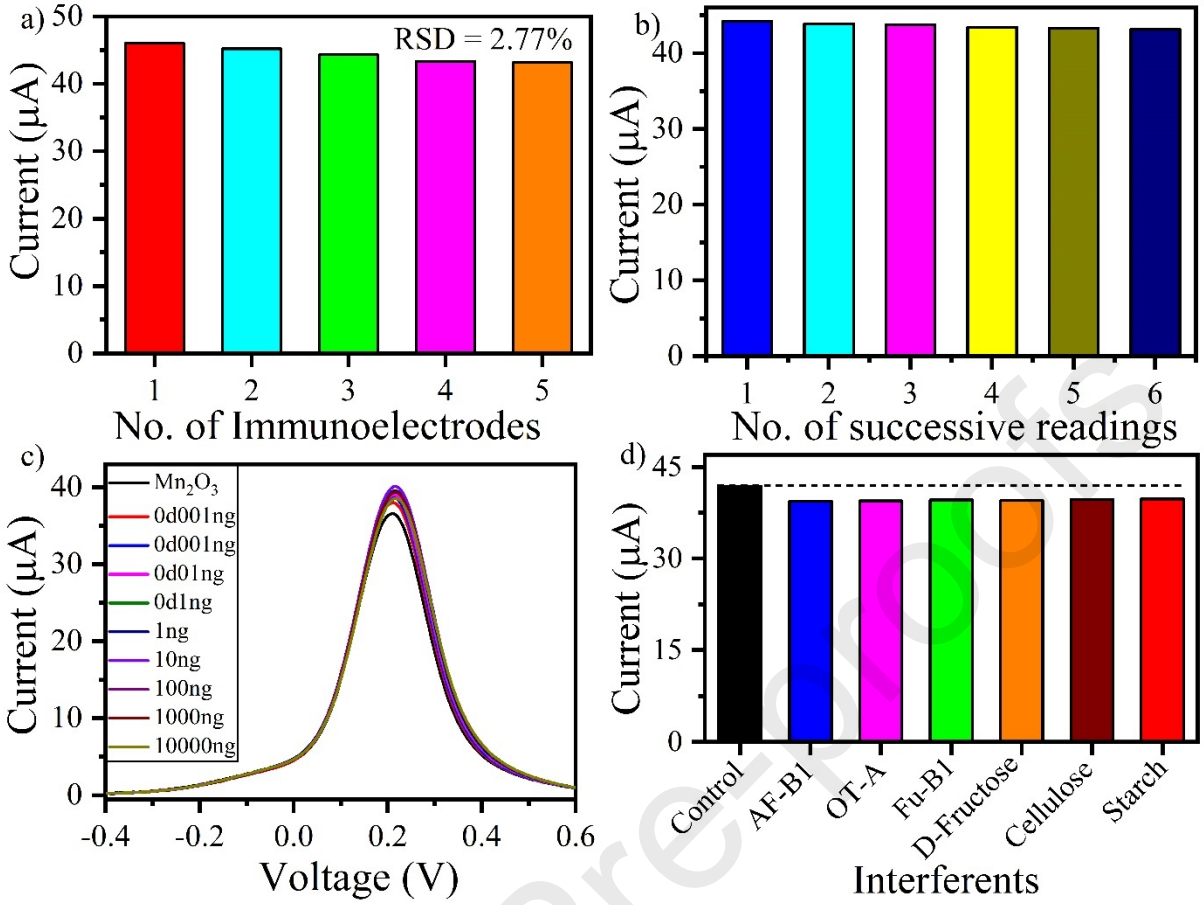

Fig. 6 (a) Reproducibility of different immunoelectrode, (b) Repeatability study of BSA/Anti-AFB1/Mn_2O_3/ITO immunoelectrode, (c) Control measurement for Mn_2O_3/ITO electrode and (d) interferant study of BSA/Anti-AFB1/Mn_2O_3/ITO immunoelectrode against several interferantsin PBS (0.1 M; 7 pH) containing $[Fe(CN)_6]^{3-/4-}$.

4. Conclusions

The Mn_2O_3 of cubic phase were synthesized using the wet-chemical co-precipitation XRD and Raman studies confirmed the formation of a pure cubic structure with the Ia3 space group. The electrophoretic deposition was used to prepare the Mn_2O_3nps film on ITO coated glass surface. Anti-AFB1 and BSA were immobilized onto Mn_2O_3/ITO electrode. FT-IR and DPV confirmed the immobilization of Anti-AFB1 and BSA onto the Mn_2O_3/ITO electrode. The BSA/Anti-AFB1/Mn_2O_3/ITO immunoelectrode was used to study the response of AFB1(standard antigen) and spiked sweet corn with AFB1 in the range of 1 pg mL^{-1} to 10 μg mL^{-1}. The immunoelectrode showed a highsensitivity of 2.044 μA mL $ng^{-1}cm^{-2}$ for AFB1

(non-spiked) samples and 1.484 μA mL $ng^{-1}cm^{-2}$ for AFB1 spiked sweet corn samples. The limit of detection (LOD) for non- spiked sample and AFB1 spiked sweet corn was found as 0.55 pg mL^{-1} and 0.58 pg mL^{-1}, respectively. The obtained recovery for sweet corn was between 95-98.6 %, which indicates the perfect applicability of the BSA/Anti-AFB1/ Mn_2O_3/ITO immunoelectrode system for the detection of AFB1 in real sample. Different interferants like other mycotoxins such as OTA and FU-B1 and chemicals such as D-fructose, cellulose, and starch that are naturally present (along with AFB1) in food items were used the interference study, in order to confirm the specific detection of AFB1. BSA/Anti-AFB1/Mn_2O_3/ITO immunoelectrode showed specific detection towards the AFB1. Furthermore, BSA/Anti-AFB1/Mn_2O_3/ITO immunoelectrodes were found behighly reproducible and repeatable for five electrodes and successive readings, respectively. In the control study, the Mn_2O_3/ITO electrode did not show any trend for the detection of AFB1, confirming the specific interaction of AFB1 with BSA/Anti-AFB1/Mn_2O_3/ITO immunoelectrode.

ORCID

Avinash K Singh: 0000-0003-3626-1643

Tarun K.Dhiman: 0000-0003-0006-7267

Lakshmi GBVS:0000-0001-7055-4533

Pratima R. Solanki: 0000-0003-1679-2180

Competing Interests

The authors declare no competing interests.

Acknowledgment

The authors are thankful to the Advanced Instrument Research Facility (AIRF) and School of Physical Science (SPS), JNU, for facilitating with the instrumentation facility. GBVSL is thankful to DST for funding through DST Women Scientist Project (SR/WOS-A/PM-

108/2016). This work was supported by a grant from the Department of Science & Technology and Department of Biotechnology (Indo- Russia Project) (DBT/IC-2/Indo-Russia/2017-19/02) Government of India.

References

1. W. Wei, X. Cui, W. Cheng, D. G. Ivey, *Chemical Society Reviews*, 2011, **40**, 1697–1721.
2. D. R. Lide, Handbook of Chemistry and Physics, CRC Press 72nd edn, 1991–1992.
3. R. B. King, Encyclopedia of inorganic chemistry, *Wiley, Chichester, New York*, 1994.
4. X. Shan, F. Guo, W. Xu, X. Teng, *Frontiers* in *Energy*, 2017, **11**, 383–400.
5. M. Wu, P. Hou, L. Dong, L. Cai, Z. Chen, M. Zhao, J. Li, *International Journal of Nanomedicine*, 2019, **14**, 4781–4800.
6. Y. Chen, H. Cong, Y. Shena, B. Yu, *Nanotechnology*, 2020.
7. Y. Qiu, G.L. Xu, K. Yan, H. Sun, J. Xiao, S. Yang, S.G. Sun, L. Jin and H. J. Deng, *Journal of Materials Chemistry*, 2011, **21**, 6346-6353.
8. S. Meng, W. Yan, X. Ma, D. Sun, Y. Jin and K. He,*RSC Advances,* 2019, **9**, 1284-1289.
9. X. Liu, C. Chen, Y. Zhao and B. Jia, *Journal of Nanomaterials,*2013, **2013**.
10. P. Ragupathy, H. Vasan and N. Munichandraiah,*Journal of the Electrochemical Society, 1*2008, **155**, A34-A40.
11. C. Cheng, Y. Huang, N. Wang, T. Ziang, S. Hu, B. Zheng, H. Yuan, D. Xiao, *ACS Applied Materials & Interfaces,* 2015,**7**(18), 9526-33.
12. P. Supraja, S. Tripathy, S. R. K. Vanjari, V. Singh, S. G. Singh, *Sensors and Actuators, B,*2019, **285**, 317-325.
13. S. Tripathy, S. Rama Krishna Vanjaria, V. Singh, S. Swaminathan, *Biosensors and Bioelectronic*, 2016, **5663**,31236-2.
14. Eaton DL, Groopman JD, editors. The toxicology of aflatoxins: human health, veterinary, and agricultural significance. *Elsevier,* 2013.
15. International Agency for Research on Cancer. Evaluation of the carcinogenic risk of chemicals to humans. Chemicals, industrial processes and industries associated with cancer in humans. 1982.
16. P. R. Solanki, J. Singh, B. Rupavali, S. Tiwari,and B. D. Malhotra, *Materials Science and Engineering C,* 2017, **70**, 564-571.
17. R. Chauhan, J. Singh, P. R. Solanki, T. Basu, R. O'Kennedy and B. D. Malhotra, *Biochemical Engineering Journal,* 2015, **103**, 103-113.
18. R. Chauhan, J. Singh, P. R. Solanki, T. Manaka, M. Iwamoto, T. Basu,and B. D. Malhotra, *Sensors and Actuators, B,* 2016, **222**, 804-814.
19. J. Singh, A. Roychoudhury, M. Srivastava, P. R. Solanki, D. W. Lee, S. H. Lee and B. D. Malhotra, *Journal of Materials Chemistry B,* 2013, **1**, 4493-4503.
20. S. Srivastava, V. Kumar, M. A. Ali, P. R. Solanki, A. Srivastava, G. Sumana, P. S. Saxena, A. G. Joshi and B. D. Malhotra,*Nanoscale,*2013, **5**, 3043-3051.
21. A. Sharma, Z. Matharu, G. Sumana, P. R. Solanki, C. Kim and B. D. Malhotra,*Thin Solid Films.,* 2010, **519**, 1213-1218.
22. P. Kalita, J. Singh, M. Kumar Singh, P. R. Solanki, G. Sumana and B. D. Malhotra, *Applied Physics Letters,* 2012, **100**, 093702.
23. H. Ma, J. Sun, Y. Zhang and S. Xia,*Biochemical Engineering Journal.,* 2016, **115**, 38-46.

24. M. V. Foguel, G. Furlan Giordano, C. M. De Sylos, I. Z. Carlos, A. A. Pupim Ferreira, A. V. Benedetti and H. Yamanaka, *Chemosensors,*2016, **4**, 17.
25. S. Zhang, Y. Shen, G. Shen, S. Wang, G. Shen and R. Yu, *Analytical Biochemistry,*2016, **494**, 10-15.
26. D. Pan, G. Li, H. Hu, H. Xue, M. Zhang, M. Zhu, X. Gong, Y. Zhang, Y. Wan, Y. Shen, *Chemistry Eur. J*, 2018,**24(39)**, 9869-9876.
27. A. Sharma, A. Kumar,and R. Khan, *Materials Science and Engineering C,* 2017, **76**, 802-809.
28. R.M. Pemberton, R. Pittson, N. Biddle, G.A. Drago and J.P. Hart, *Analytical letters*, 2006, 39,1573.
29. Y. Tan, X. Chu, G.L. Shen and R.Q. Yu, *Analytical Biochemistry,* 2009, **387**, 82-86.
30. G. Evtugyn, A. Porfireva, V. Stepanova, R. Sitdikov, I. Stoikov, D. Nikolelis and T. Hianik, *Electroanalysis.*, 2014, **26**, 2100-2109.
31. T. K. Dhiman, G. Lakshmi, A. Roychoudhury, S. K. Jha and P. R. Solanki, *Chemistry Select,* 2019, **4**, 4867-4873.
32. T. Sarkar, T. K. Dhiman, R. Sajwan, S. Sri, P. R. Solanki. *Nanotechnology*. 2020.**31,** 355502 (12pp).
33. T.K. Dhiman, G. Lakshmi, R. Kumar, K. Asokan, P. R. Solanki. *IEEE Sensors Journal.* 2020.
34. A. K. Yadav, T. K. Dhiman, G. Lakshmi, A. N. Berlina and P. R. Solanki, *International Journal of Biological Macromolecules,* 2020, **151**, 566-575.
35. J. Conde, J. T. Dias, V. Grazú, M. Moros, P. V. Baptista, J. M. de la Fuente, *Frontiers in Chemistry,* 2014, **2**, 48.
36. N. Pachauri, G. Lakshmi, S. Sri, P. K. Gupta,and P. R. Solanki, *Materials Science and Engineering* C*,* 2020, 110911.
37. W. B. White and V. G. Keramidas, *Spectrochimica Acta, Part A*, 1972, **28**, 501-509.
38. S. H. Shim, D. LaBounty, and T. S. Duffy, *Physics and Chemistry of Minerals,* 2011, **38**, 685.
39. T. Gao, M. Glerup, F. Krumeich, R. Nesper, H. Fjellvåg and P. Norby, *Journal of Physical Chemistry C,* 2008, **112**, 13134-13140.
40. H. R. Barai, A. N. Banerjee, N. Hamnabard and S. W. Joo, *RSC Advances,* 2016, **6**, 78887-78908.
41. F. Kapteijn, A. D. Vanlangeveld, J. A. Moulijn, A. Andreini, M. A. Vuurman, A. M. Turek, J. M. Jehng and I. E. Wachs, *Journal of Catalysis,*1994, **150**, 94-104.
42. D. T. Zahn,*Physical Chemistry Chemical Physics,* 1999, **1**, 185-190.
43. M. Mylarappa, V. V. Lakshmi, K. V. Mahesh, H. Nagaswarupa and N. Raghavendra, *Materials Science and Engineering,* 2016, 149, **1**, 012178.
44. L. Kang, M. Zhang, Z. H. Liu,and K. Ooi, *Spectrochimica Acta Part A,* 2007, **67**, 864-869.
45. J. Chalmers and P. Griffiths, *Handbook of Vibrational Spectroscopy, 5 volumes set*, Wiley, 2002.
46. S. Tiwari, P. K. Gupta, Y. Bagbi, T. Sarkar, and P. R. Solanki, *Biosensors and Bioelectronics*, 2017, **89**, 1042-1052.
47. P. K. Gupta, Z. H. Khan and P. R. Solanki, *Journal of Electroanalytical Chemistry,* 2018, **829**, 69-80.

Highlights

- Manganese oxide nanoparticles (Mn_2O_3nps) based electrochemical immunosensor was reported for Aflatoxin-B1 detection.
- Pure phase Mn_2O_3nps were obtained at 550 ^oC without going for high calcination temperature.
- The immunoelectrode showed a high sensitivity with better LOD and good selectivity.
- Spiked sample study of corn extract showed a very good linear response with up to 98.6 % recovery.